Tomonaga-Luttinger liquid parameters of magnetic waveguides in graphene

Wolfgang Häusler, A. De Martino, T. K. Ghosh, Reinhold Egger

Angaben zur Veröffentlichung / Publication details:

Häusler, Wolfgang, A. De Martino, T. K. Ghosh, and Reinhold Egger. 2008. "Tomonaga-Luttinger liquid parameters of magnetic waveguides in graphene." *Physical Review B* 78 (16): 165402. https://doi.org/10.1103/physrevb.78.165402.

Tomonaga-Luttinger liquid parameters of magnetic waveguides in graphene

W. Häusler,[1,2] A. De Martino,[1,3] T. K. Ghosh,[1,4] and R. Egger[1]
[1]*Institut für Theoretische Physik, Heinrich-Heine-Universität, D-40225 Düsseldorf, Germany*
[2]*Physikalisches Institut, Albert-Ludwigs-Universität, D-79104 Freiburg, Germany*
[3]*Institut für Theoretische Physik, Universität zu Köln, Zülpicher Strasse 77, D-50937 Köln, Germany*
[4]*Department of Physics, Indian Institute of Technology-Kanpur, Kanpur 208016, India*
(Received 16 July 2008; published 2 October 2008)

Electronic waveguides in graphene formed by counterpropagating snake states in suitable inhomogeneous magnetic fields are shown to constitute a realization of a Tomonaga-Luttinger liquid. Due to the spatial separation of the right- and left-moving snake states, this non-Fermi liquid state induced by electron-electron interactions is essentially unaffected by disorder. We calculate the interaction parameters accounting for the absence of Galilei invariance in this system, and thereby demonstrate that non-Fermi liquid effects are significant and tunable in realistic geometries.

DOI: 10.1103/PhysRevB.78.165402 PACS number(s): 71.10.Pm, 73.21.−b, 73.63.−b

I. INTRODUCTION

One-dimensional (1D) electron systems can nowadays be studied in different material systems, e.g., by depositing negatively charged metallic gate electrodes on top of a two-dimensional electron gas (2DEG) in semiconducting heterostructures, thereby depleting the 2DEG to form the desired structure,[1] or in single-wall nanotubes (SWNTs).[2] Such 1D quantum wires have been argued to realize the non-Fermi liquid behavior of a Tomonaga-Luttinger liquid (TLL),[3–7] arising as a consequence of electron-electron (*e-e*) interactions. Experimental signatures of TLL behavior include nonuniversal power laws in certain transport properties related to the tunneling density of states, but many other observables also may reflect the non-Fermi liquid properties of a TLL. Experimental observations in semiconductor quantum wires[8] were explained by TLL parameters of the order of $g_c \approx 0.4$ to 0.5, while the corresponding parameter in SWNTs[9] was reported as $g_{c+} \approx 0.16$ to 0.3. Both values are significantly smaller than the respective noninteracting value, $g=1$.

Very recently, graphene monolayers[10,11] have become available as a new realization of a 2DEG, albeit with properties strikingly different from their semiconducting counterparts. The kinetic energy of graphene close to one of the Dirac (K,K') points is described by a two-component chiral Dirac-Weyl Hamiltonian[12,13]

$$H = v_F \boldsymbol{\tau} \cdot (\mathbf{p} - \mathbf{A}) \tag{1}$$

of massless relativistic particles moving at graphene's Fermi velocity $v_F \approx 10^6$ m/sec, instead of the usual Schrödinger Hamiltonian $\mathbf{p}^2/2m^*$ (with effective mass m^*). In Eq. (1), $\boldsymbol{\tau}$ denotes the vector of Pauli matrices in sublattice ("pseudospin") space, while the physical spin, as well as the valley $(K-K')$ degrees of freedom, are left implicit. Furthermore, we have allowed for a static inhomogeneous orbital magnetic field perpendicular to the graphene plane (the field components in the plane do not affect orbital motion), $\mathbf{B} = B(x,y)\hat{e}_z$, which is incorporated by minimal (Peierls) coupling in terms of the corresponding vector potential $\mathbf{A}(x,y)$. This gives rise to interesting magnetic barrier and magnetic confinement effects.[14–17]

It is well known, both theoretically[18] and experimentally,[19] that a magnetic-field gradient can give rise to unidirectional 1D snake states. Such orbits were recently studied theoretically in graphene[20–22] and in SWNTs.[23] Snake states carry current along the lines where the magnetic field changes sign, and hence is zero. On a classical level, they can be understood as half orbits of different circulation sense (for $B>0$ and $B<0$), patched together to form a unidirectionally propagating orbit.[24] Pairs of snake states running antiparallel to each other are referred to as double-snake states.[25] In many regards, double-snake states correspond to the standard left and right movers in 1D quantum wires. For example, they should exhibit quantized conductance in multiples of $4e^2/h$ (including spin and valley degeneracies). Since the snake states are spatially separated, this quantization should be robust: shallow impurities are not expected to cause scattering between snake modes of opposite directionality.

In this work, we address consequences of the long-ranged but ultimately screened *e-e* interactions within and between the counterpropagating snake orbits in graphene magnetic waveguides. For a wide class of experimentally relevant field profiles, we show that a TLL state with broken Galilei invariance and extremely weak disorder sensitivity can be realized. On a general level, the importance of *e-e* interactions for the correct interpretation of experimental data in graphene has recently been stressed.[26] Theories describing *e-e* interaction effects on the transport properties of electrons in graphene have been proposed for strong homogeneous magnetic fields[27] and for zero magnetic field.[28] A recent debate has discussed the question whether interacting electrons in undoped graphene form a Fermi liquid or not.[29,30] Interactions are also predicted to yield a TLL state in special graphene nanoribbons with armchair edges.[31]

For the related case of interacting metallic SWNTs, the effective low-energy theory predicts a four-channel TLL state,[32,33] where the spin and valley degrees of freedom give rise to the four channels. There is one charged $(c+)$ channel, where the long-ranged *e-e* interactions play a crucial role, while the three neutral channels are basically insensitive to interactions. We will see that the situation in a graphene magnetic waveguide is similar, and the parameter g dis-

cussed below plays the role of the SWNT parameter g_{c+}. Albeit the interaction does not spoil conductance quantization in dc transport for adiabatically connected reservoirs,[34] it nevertheless destroys the Fermi-liquid character of the system. In fact, it leads to nonuniversal power laws in the tunneling density of states, and to peculiar ac transport and shot noise[35] properties at low temperatures. These phenomena are appropriately described by TLL theory.[3–7] The respective power-law exponents can be directly inferred from Refs. 32 and 33 by simply replacing g_{c+} with our estimate for g [see Eq. (32) below].

After introducing the model and the magnetic-field profiles in Sec. II A, the band structure is studied in Gaussian approximation in what follows in Sec. II B. The analytical band structure results are validated by comparing to exact diagonalization results. The numerical diagonalization is briefly discussed in Appendix. The linearized band structure for a double-snake state waveguide leading to TLL behavior is then described in Sec. III A. The physics of a TLL is governed by a dimensionless interaction parameter g, for which general expressions in terms of certain velocities are derived in Sec. III B. These velocities are obtained from perturbative expressions for the ground-state energy, and yield the analytical results for g given in Sec. IV. We conclude in Sec. V. In Secs. III and IV, to be specific, we focus on electron-like excitations by assuming a positive value of the Fermi energy ε_F. Below, we often take units such that $\hbar = v_F = 1$.

II. MODEL AND BANDSTRUCTURE

A. Model

In this paper, we consider magnetic fields $B=B(x)$, guiding particles homogeneously along the y direction. This implies that the wave number k along this direction is conserved. Two-component eigenstates of the Dirac-Weyl Hamiltonian [Eq. (1)] can then be written as $\psi(x,y) \sim e^{iky}(\phi_k(x),\chi_k(x))^T$. The vector potential can be chosen as $\mathbf{A}=A(x)\hat{e}_y$, with the spinor components obeying

$$\begin{pmatrix} 0 & -i\partial_x - ik + iA(x) \\ -i\partial_x + ik - iA(x) & 0 \end{pmatrix} \begin{pmatrix} \phi_k(x) \\ \chi_k(x) \end{pmatrix} = \varepsilon_k \begin{pmatrix} \phi_k(x) \\ \chi_k(x) \end{pmatrix}. \tag{2}$$

Complex phases may be chosen such that ϕ_k is real and χ_k purely imaginary. After squaring, Eq. (2) can be cast into a Schrödinger-type form for the upper Dirac component ϕ_k,

$$[-\partial_x^2 + [k - A(x)]^2 - B(x) - \varepsilon_k^2]\phi_k(x) = 0. \tag{3}$$

A similar equation holds for the lower component $\chi_k(x)$, with the sign of the "pseudo-Zeeman" term $\sim B$ reversed. Unless $\varepsilon_k=0$, Eq. (2) implies

$$\int dx |\phi_k(x)|^2 = \int dx |\chi_k(x)|^2 = 1/2. \tag{4}$$

Note that in path-integral approaches to relativistic quantum mechanics, in order to guarantee convergence of the Wiener measure,[36] often the square of the Dirac Hamiltonian [Eq. (1)] is considered. Path-integral representations, on the other hand, allow for systematic approximations, and therefore, Eq. (3) is a useful starting point for the Gaussian approximation, cf. Sec. II B, where the boundedness of the differential operator appearing in Eq. (3) is exploited for either sign of $B(x)$, in the spirit of a saddle-point approximation. Our method differs from Wentzel-Kramers-Brillouin (WKB)-type approaches recently put forward to describe the electronic properties of graphene.[22,37] We note in passing that massive Schrödinger particles obey a related equation as Eq. (3), with quadratic momenta multiplied by $1/(2m^*)$, in the same magnetic-field profile; only the pseudo-Zeeman term must be removed, and of course, the energy ε_k^2 must be replaced by ε_k, i.e., hole and zero-energy states both disappear. As a consequence, most of our conclusions also apply (at least qualitatively) to magnetic waveguides based on traditional Schrödinger fermions.

We consider the class of magnetic-field profiles given by

$$B(x) = \nu\omega_B(\sqrt{\omega_B}x)^{\nu-1} - B_0. \tag{5}$$

In our gauge, we thus have

$$A(x) = \omega_B^{\frac{\nu+1}{2}} x^\nu - B_0 x. \tag{6}$$

The index ν can describe rather different situations, but we are only interested in ν being a natural number. For instance, for $\nu=1$, we recover the homogeneous magnetic-field case, giving rise to the standard relativistic Landau levels. For $\nu=2$, profile (5) instead describes a setup with one snake state propagating along the y direction, while $\nu=3$ (or, more generally, all odd $\nu>1$) can give rise to a double-snake state geometry, where the background magnetic field $-B_0$ allows for lines with $B=0$, and ω_B sets the inhomogeneity scale. Equation (3) manifests the electron-hole symmetry $\varepsilon_k \leftrightarrow -\varepsilon_k$ of Eq. (2), with a zero-energy eigenstate ($\varepsilon_k=0$ for all k) appearing whenever ν is odd, but not for even ν.[38]

Equation (5) qualitatively describes many situations of experimental relevance, where typically smooth magnetic-field profiles are present. Of course, far away from the waveguide defined by the snake states, the actual profile is different in practice, but this does not significantly affect the TLL discussed below. In fact, we have also analyzed step-like field profiles, such as the ones described in Ref. 21, with very similar results and conclusions. For $\nu=3$, counterpropagating snake states are centered around $x=\pm d$ with $B(\pm d)=0$, leading to

$$d = \frac{\sqrt{B_0}}{\sqrt{3}\omega_B}, \tag{7}$$

such that $2d$ is the parallel distance between counterpropagating snake states. In this configuration, a TLL can be realized, and most of our analysis will deal with this case.

Below, we will ignore the Zeeman splitting due to the interaction of the true electronic spin with the magnetic field creating the waveguide. A simple estimate for a homogeneous magnetic field already shows that this approximation is justified in graphene. The physical Zeeman splitting $\Delta_Z = g_e\mu_B B$ amounts to 0.116 meV for $B=1$ Tesla, taking $g_e=2$ and the free electron mass m_e going into Bohr's magne-

ton μ_B. This value can be compared to the orbital splitting $\Delta_{\rm orb}$ between subsequent levels—in the language of Eq. (3), this corresponds to a "pseudo-Zeeman splitting"—with the result

$$\frac{\Delta_Z}{\Delta_{\rm orb}} \simeq \frac{\varepsilon_F}{m_e v_F^2}, \tag{8}$$

predicting that even for $\varepsilon_F = 1$ eV, the Zeeman splitting is 50 times smaller than the orbital splitting. In view of the smallness of ratio (8), we will neglect Zeeman terms in what follows. In any case, their effects on the low-energy theory of interacting electrons in graphene waveguides are standard and could be included along the lines of Refs. 4–7.

B. Gaussian approximation

Next we describe our analytical approach to the band structure and the eigenfunctions. They allow for closed form expressions of the TLL parameter g in Sec. IV. At large $|k|$, when anharmonic contributions of the effective potential appearing in Eq. (3) are suppressed, the Gaussian approximation becomes exact. To confirm the accuracy of the analytical results, we have carried out numerical diagonalizations of the matrix representing the Schrödinger-type Hamiltonian [Eq. (3)] in a complete basis set. This is briefly described in Appendix.

It is instructive to first study one of the two counterpropagating snake modes individually. We therefore set $B_0 = 0$ and $\nu = 2$ in Eq. (5), i.e., $B(\xi) = 2\omega_B \xi$ with $\omega_B > 0$, where we introduce dimensionless lengths, $\xi = \sqrt{\omega_B} x$, and momenta, $\kappa = k/\sqrt{\omega_B}$. The Schrödinger version of this model has been studied previously.[18] The single-snake state is now centered near $x = 0$ with (positively or negatively charged) particles running in the negative y direction. The spectrum in this case is not symmetric, $\varepsilon_k \neq \varepsilon_{-k}$. We then need to discuss the effective potential appearing in Eq. (3),

$$V_{\nu=2}(\kappa, \xi) = (\xi^2 - \kappa)^2 - 2\tau_z \xi,$$

which depends on the sublattice component $\tau_z = \pm 1$ of the wave function. Obviously, for any κ, $V_{\nu=2}$ is invariant under the combined operation $\tau_z \to -\tau_z$ and $\xi \to -\xi$ so that $|\phi_k(\xi)| = |\chi_k(-\xi)|$ in Eq. (2). For $\kappa \to -\infty$, the minima of $V_{\nu=2}$ approach κ^2 at $\xi = 0$ so that $|\phi_k(\xi)| = |\chi_k(\xi)| \sim e^{-\sqrt{-\kappa/2}\xi^2}$ and $\varepsilon_{k \to -\infty} \to -k$. This indicates that the velocity reaches, up to subleading corrections, the negative of the Fermi velocity. This is precisely the snake state with both components of the Dirac spinor localized near $x = 0$. In the other limit, $\kappa \to +\infty$, the minima of $V_{\nu=2}$ approach $-2\sqrt{\kappa}$ at $\xi = \tau_z \sqrt{\kappa}$. In that case, the two sublattice components $|\phi_k(\xi)| = |\chi_k(-\xi)| \sim e^{-\sqrt{\kappa}[\xi - \sqrt{\kappa}]^2}$ are spatially separated from one another and from the snake mode, provided the distance exceeds the widths of these distributions. This result suggests an interesting application as a "sublattice filter," where the magnetic field leads to a spatial separation of particles located on different sublattices. However, for the other K point, the sublattice states are exchanged, and in order to see such an effect, one would need to have a valley-polarized system (i.e., a single K point). The corresponding energy in Gaussian approximation is $\varepsilon_{k \to +\infty} \to 0$. This result cannot be recovered using WKB-type approaches,[22,37] which are more suited to describe higher excited states. Interestingly, the positions $\xi = \pm\sqrt{\kappa}$ of these states remain protected against the pseudo-Zeeman field "inclination" from Eq. (3), contrary to naive expectation and in contrast to the nonzero shift found in any of the excited states. Finally, also excited energies can be estimated in this way. For example, the first excited level is expected at $\varepsilon_k = 2\omega_B^{3/8} k^{1/4}$.

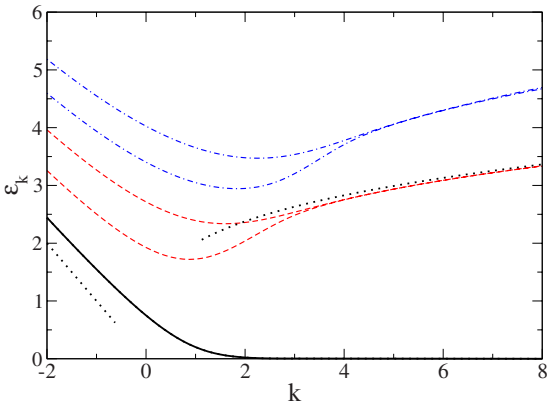

FIG. 1. (Color online) Electron-like energy eigenvalues ε_k versus momentum k (both in units of $\sqrt{\omega_B}$), as obtained by numerical diagonalization of Eq. (3) for a magnetic-field profile with $\nu = 2$ and $B_0 = 0$ in Eq. (5). The solid (black) curve denotes the lowest positive-energy eigenstate, and the dashed (red) and dash-dotted (blue) curves give the next two pairs of excited states. The dotted curve indicates the limiting snake-state dispersion $\varepsilon_k = -k$ for $k < 0$, and the result in Gaussian approximation for the first excited energy band, $\varepsilon_k = 2\omega_B^{3/8} k^{1/4}$, for $k > 0$. Note that for the lowest state, $\varepsilon_{k \to +\infty}$ approaches zero energy (Refs. 20 and 21), in agreement with the Gaussian approximation.

In effect, we then arrive at a picture where snake (near $x = 0$) and "bulk" modes (near $x = \pm\omega_B^{-3/4}\sqrt{k}$) will develop. We here distinguish "snake" and "bulk" modes by their respective group velocities. Figure 1 clearly demonstrates how the eigenstates evolve from snake states (at $k \to -\infty$ with $\partial_k \varepsilon_k = -1$) into bulk modes at $k \to +\infty$. In Fig. 2 the corresponding metamorphosis is displayed of a (single) snake state at sufficiently negative k centered around $\xi = 0$ [see Fig. 2(a)], into a bulk state, residing increasingly far away from $\xi = 0$ with increasing $k > 0$. For $\kappa = 8$, cf. Fig. 2(b), the state is located near $\xi = 2.83\tau_z$ as expected.

Let us now turn to the magnetic-field profile with $\nu = 3$ in Eq. (5), which should exhibit double-snake states of opposite directionality due to the existence of two zeros of $B(x)$. To some extent, we now have two copies of the above single-snake state situation at a distance $2d$ [cf. Equation (7)]. Since $B(x) = B(-x)$, the dispersion relation is now symmetric, $\varepsilon_k = \varepsilon_{-k}$. At $k \to \pm\infty$, we thus anticipate the coexistence of snake and bulk modes. In addition, an exact zero-energy eigenstate, $\varepsilon_k = 0$, must now occur as a consequence of the index theorem.[38] The potential entering Eq. (3) is

$$V_{\nu=3}(\kappa, \xi) = (\xi^3 - b_0 \xi - \kappa)^2 - \tau_z (3\xi^2 - b_0), \tag{9}$$

where $b_0 = B_0/\omega_B$. This potential is invariant under a simultaneous sign change of κ and ξ, transforming left-movers

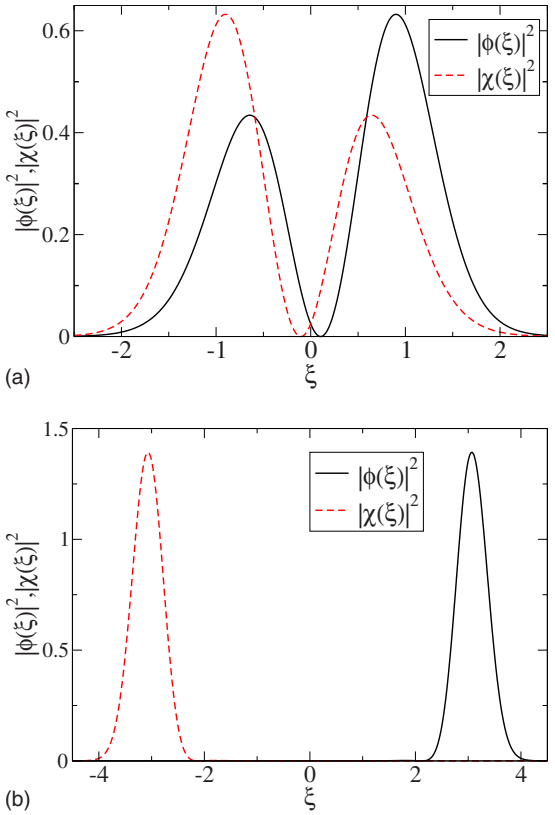

FIG. 2. (Color online) Numerical diagonalization results for the probability densities of the spinor components $|\phi_\kappa(\xi)|^2$ (black solid curve) and $|\chi_\kappa(\xi)|^2$ (red dashed curve) of the lowest eigenstate to positive energy of Eq. (2) with $\nu=2$ and $B_0=0$. (a) is for momentum $\kappa=-2$, and (b) for $\kappa=8$.

into right-movers and vice versa. Similar as for $\nu=2$, we can obtain energies in Gaussian approximation. The lowest energy, only for $\tau_z=+1$, equals zero at large $|k|$. This describes the zero-energy state, present for any k at odd ν (cf. Sec. II A and Appendix). The first excited (positive) energy is approximated as

$$\varepsilon_k = \sqrt{6}|\omega_B k|^{1/3} + B_0/[\sqrt{6}|\omega_B k|^{1/3}]. \tag{10}$$

This result is included to the numerically obtained spectra (see Fig. 3). The corresponding eigenstates are localized around $\xi=(|\kappa|^{1/3}+b_0/3|\kappa|^{1/3}+\tau_z/3|\kappa|)\mathrm{sgn}(\kappa)$, i.e., increasingly deep in the system's bulk with increasing $|k|$. Figure 3 shows a typical spectrum obtained from numerical diagonalization. Depending on the slopes $\partial_k\varepsilon_k$ at large $|k|$, one type of band goes like $\varepsilon_k \simeq \pm v_F|k|$, corresponding to the counterpropagating snake states centered around $x=\pm d$ [see Eq. (7)]. Snake states move with the Fermi velocity of graphene at large $|k|$, irrespective of the magnetic-field profile.[20,21,39] The other bands in Fig. 3 exhibit smaller slopes at large $|k|$. The corresponding states are localized increasingly further away from the center of the wire at increasing $|k|$, and we thus call them again "bulk" modes. Due to their different slopes, bands of different types should cross, and Fig. 3 indeed reveals avoided intersections. Such avoided level crossings can be attributed to some residual hybridization between

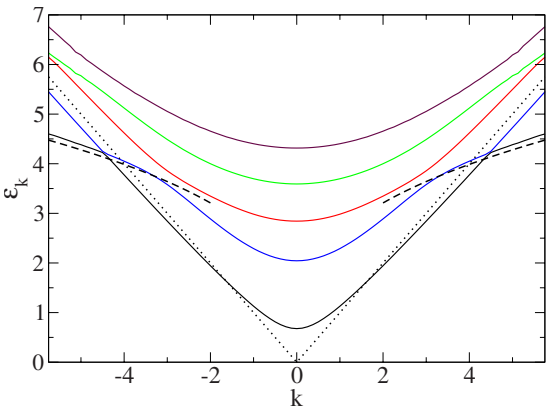

FIG. 3. (Color online) Same as Fig. 1 but for $\nu=3$ and $B_0=1.526\omega_B$. Full curves (in different colors) give the numerical diagonalization results for the eigenenergies. When the Fermi level intersects only the lowest (black) curve, one has precisely one (spin- and valley-degenerate) left- and right-moving state in the waveguide. This leads to a TLL state. The dotted curve denotes $\varepsilon_k=|k|$, and the dashed curve gives the estimate (10) for the lowest dispersing energy band in the Gaussian approximation.

snake and bulk modes. They become successively less important as the bulk state's center moves away from the snake state with increasing $|k|$.

Figure 4 validates the behavior of the two types of eigenstates for the double-snake $\nu=3$ situation with $\kappa=-6$. In view of Fig. 3, this value of $|\kappa|$ is just beyond one of the (narrower) avoided crossings so that the lowest positive-energy state, exhibiting a moderate slope, must be identified as a bulk state. This is indeed confirmed in Fig. 4, where the densities of both components of this state are seen. Gaussian approximation predicts its center to be at $\xi=-2.1+0.06\tau_z$, which is nicely confirmed by comparing to exact diagonalization results. The first excited state at $\kappa=-6$ has $\partial_k\varepsilon_k \simeq -1$, and therefore is classified as snake state. Indeed, as seen in Fig. 4, both pseudospin components of this state reside near $\xi=0.7$, where $B(\xi)=0$. Note that, according to Eq. (22), densities for odd ν are mirror symmetric under simultaneous sign reversal of κ and ξ so that the $\kappa=+6$ state is centered at $\xi=-0.7$. Finally, we note that all densities in Figs. 2 and 4

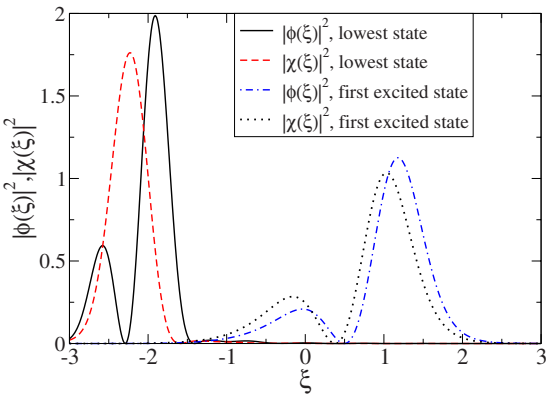

FIG. 4. (Color online) Same as Fig. 2 but for a magnetic field (5) with $\nu=3$ and $B_0=1.525\omega_B$. Shown are the two lowest positive-energy eigenstates with $\kappa=-6$.

are well approximated by superpositions of suitable Gaussians, in accordance with our Gaussian description.

III. INTERACTION EFFECTS

A. Waveguide model

When considering a 1D graphene magnetic waveguide with counterpropagating snake states at low-energy scales, see Sec. II B, the question arises whether *interacting* Dirac fermions in such a waveguide belong to the TLL universality class.[3–7] As always happens in 1D, Landau quasiparticles will be destroyed by any nonzero *e-e* interaction strength,[40] but whether the resulting non-Fermi liquid is a TLL remains to be shown. Indeed, this expectation is corroborated by the analogous situation in a quantum Hall bar,[41,42] where, as a consequence of the long-ranged Coulomb interaction between different edge states, a TLL with spatially separated left- and right-moving edge states emerges.[43]

We start with a discussion of the relevant single-particle band structure. For a magnetic waveguide with $\nu=3$ and $B_0>0$ in Eq. (5), the lowest positive-energy subband $\varepsilon_k^{(1)}=\varepsilon_{-k}^{(1)}$ has left- and right-going snake states near $x=\pm d$ [see Eq. (7)] that essentially move at velocity $\pm v_F$. We assume that the Fermi level intersects these states at $\pm k_F$, and that all other states are energetically sufficiently far away. This band structure was discussed in detail in Sec. II B (see Fig. 3). Using second quantization, the kinetic energy is then described by

$$H_0=\sum_k \varepsilon_k^{(1)} c_k^\dagger c_k, \tag{11}$$

where $c_k^\dagger$ (c_k) creates (annihilates) a Dirac quasiparticle with momentum k, and spin and valley indices are kept implicit. The electron field operator for waveguide length L along the y direction is thus written as

$$\Psi(x,y)=\frac{1}{\sqrt{L}}\sum_k e^{iky}\begin{pmatrix}\phi_k(x)\\ \chi_k(x)\end{pmatrix}c_k. \tag{12}$$

The crucial parameters characterizing the TLL are certain velocities.[5] In the noninteracting case, Dirac particles move at velocity[21]

$$v_F\langle\tau_y\rangle_k=2v_F\,\mathrm{Im}\int dx\phi_k^*(x)\chi_k(x)=\partial_k\varepsilon_k\equiv v_k,$$

given by the slope of the energy dispersion, just as for Schrödinger particles. Assuming that ε_F is sufficiently far away from both the band bottom of $\varepsilon_k^{(1)}$ and from the next-higher energy band, we linearize $\varepsilon_k^{(1)}$ about the two Fermi points $k=\pm k_F$, yielding velocities $\pm v_{k_F}$. This also separates right ($k>0$) from left ($k<0$) movers in Eq. (11), and implicitly defines the standard bandwidth cutoff around the Fermi level used in TLL theory.

B. Tomonaga-Luttinger liquid

Next we incorporate *e-e* interactions within an effective low-energy theory. We consider the pair interaction potential[44]

$$W(\mathbf{x}_1,\mathbf{x}_2)=\frac{e^2}{\kappa_0}\left(\frac{1}{|\mathbf{x}_1-\mathbf{x}_2|}-\frac{1}{\sqrt{(\mathbf{x}_1-\mathbf{x}_2)^2+4D^2}}\right) \tag{13}$$

between electrons at coordinates $\mathbf{x}_1=(x_1,y_1)$ and $\mathbf{x}_2=(x_2,y_2)$. This form specifically accounts for screening by metal gates positioned at some distance D from the waveguide. Its strength is governed by the dimensionless "fine structure constant" $\alpha=e^2/[\kappa_0\hbar v_F]$, which basically depends only on the dielectric constant κ_0. For typical substrate materials, one has values $\kappa_0\approx 1.4$ to 4.7, resulting in $\alpha\approx 0.6$ to 2.[33,45,46] For graphene, both the kinetic as well as the Coulomb energy scale ($\sim\sqrt{n}$ for particle density n) in the same way.[46] The resulting weak tunability of the *e-e* interaction strength in graphene is in stark contrast to the situation in semiconductors, where n allows to alter the relative strength of Coulomb interactions over orders of magnitude.

When constructing a low-energy theory for interacting Dirac fermions in the double-snake state waveguide of Sec. III A, the resulting 1D *e-e* interaction processes can be classified as forward-scattering and backscattering processes.[3–7] The spatial separation of the unidirectional snake states here implies a strong suppression of *e-e* backscattering processes, where the relevant couplings are exponentially small in the parameter $k_F d\gg 1$. In the following, we discuss the regime

$$k_F D\gg k_F d\gg 1, \tag{14}$$

where backscattering processes are negligible. This situation is reminiscent of the SWNT case,[33] where one, however, finds only an algebraic suppression of the backscattering couplings with increasing SWNT radius. We then only need to include forward-scattering processes (see also Ref. 33), and arrive at a four-channel TLL model. The three neutral sectors involve spin and valley degrees of freedom and are decoupled from each other and from the charge sector (spin-charge separation). For not too strong interactions, as expected in graphene, the neutral sectors will remain basically unaffected by interactions, with their velocity parameters (almost) equal to v_{k_F} (see also Ref. 47). This implies that the TLL parameters for the three neutral sectors are just given by the noninteracting value ($g=1$). In the following, we then focus on the charge ($c+$) sector only.

The resulting TLL is most conveniently described by Abelian bosonization.[4–7,33] For the $c+$ sector, the resulting Hamiltonian is

$$H_{c+}=\frac{1}{2}\int dy[v_J[\partial_y\Theta(y)]^2+v_N[\partial_y\Phi(y)]^2], \tag{15}$$

with bosonic fields subject to the algebra $[\Phi(y),\partial_y\Theta(y)]=i\delta(y-y')$. Equation (15) reflects the fact that density waves (in contrast to quasiparticles) are undamped in a TLL.[40] With Eq. (15) and the usual bosonized form of the Fermi operators,[6] almost any observable of physical interest can be determined exactly at low energies and long wavelengths, where the TLL model applies. In general, $v_J<v_N$ can deviate from v_{k_F} as a result of the repulsive *e-e* interactions. Interaction physics is thus encoded in v_J and v_N. These velocities determine the dimensionless TLL interaction parameter $g\equiv g_{c+}$ and the plasmon velocity v according to[4]

$$g = \sqrt{v_J/v_N}, \quad v = \sqrt{v_J v_N}. \tag{16}$$

In principle, both parameters are experimentally accessible, e.g., through the tunneling density of states,[9] momentum-resolved tunneling,[8] or via plasmon propagation times.[48]

The velocities v_J and v_N can be extracted in an elegant and exact manner from thermodynamic relations,[5,49]

$$v_N = \frac{\pi}{4L}\frac{\partial^2 E_0}{\partial k_0^2}, \quad v_J = \frac{\pi}{4L}\frac{\partial^2 E_0}{\partial \delta^2}, \tag{17}$$

provided the fully interacting ground-state energy density E_0/L for fixed left $(-k_F^{(-)})$ and right $(k_F^{(+)})$ Fermi momenta is known, where $\delta=(k_F^{(+)}-k_F^{(-)})/2$ and $k_0=(k_F^{(+)}+k_F^{(-)})/2$. The derivatives in Eq. (17) are evaluated at $\delta=0$ and $k_0=k_F$, and the energy E_0 includes the spin and valley degrees of freedom. Clearly, v_N is proportional to the compressibility, and when Galilei invariance is realized, $v_J=v_{k_F}$ is unchanged by interactions. However, as we shall see below, this symmetry is *not* obeyed here due to the periodic superstructure imposed by the snake orbit.

IV. TLL PARAMETER

Unfortunately, exact results for E_0 are known only for a limited number of integrable models, such as the Hubbard model[50] or the Sutherland model.[51] Even then, one still has to numerically solve coupled pairs of integral equations to access E_0, and hence the velocities $v_{J,N}$ in Eq. (17). In actual calculations of v_J and v_N for nonintegrable models (which is the case here), one has to resort to approximations.[44,52]

A. Perturbation theory

We now use perturbation theory to obtain E_0, and thus velocities (17), for relatively weak interactions. This approximation is almost exclusively used in the literature in order to obtain estimates for the TLL parameters of generic interacting one-dimensional (1D) fermion systems. In that case, the ground-state energy can be split into three terms,

$$E_0 = E_{\rm kin} + E_{\rm Hartree} - E_{\rm Fock}, \tag{18}$$

from which several contributions to the susceptibilities [Eq. (17)] follow. Accounting for spin and valley degeneracy, we have

$$\frac{\partial^2 E_{\rm kin}}{\partial k_0^2} = \frac{\partial^2 E_{\rm kin}}{\partial \delta^2} = \frac{2L}{\pi}(\partial_k \varepsilon^{(1)}_{k_F} - \partial_k \varepsilon^{(1)}_{-k_F}) = \frac{4L}{\pi} v_{k_F}, \tag{19}$$

as expected for noninteracting quasiparticles with velocities $\pm v_{k_F}$.

From the Hartree interaction term, we then obtain

$$\frac{\partial^2 E_{\rm Hartree}}{\partial k_0^2} = \frac{L}{\pi^2}[\eta(k_F,k_F) + \eta(k_F,-k_F) + \mathcal{R}], \tag{20}$$

where, including again both spin and valley components, we define

$$\eta(k,k') = \eta(k',k) = 8\int dx \int dx' n_k(x) n_{k'}(x') \times \alpha \ln\sqrt{1+[2D/(x-x')]^2}, \tag{21}$$

with the particle density for wave vector k at location x,

$$n_k(x) = |\phi_k(x)|^2 + |\chi_k(x)|^2 = n_{-k}(-x). \tag{22}$$

Note that $\int dx n_k(x)=1$ [see Eq. (4)]. Furthermore, we have introduced the quantity

$$\mathcal{R} = \int_{-k_F}^{k_F} dk \partial_{k_F}[\eta(k,k_F) + \eta(k,-k_F)] = 2\int_0^{k_F} dk \partial_{k_F}[\eta(k,k_F) + \eta(k,-k_F)]. \tag{23}$$

The second equalities in Eqs. (22) and (23) are valid for all odd $\nu>1$. In Eq. (21), we have used that only long wavelengths $q\to 0$ are important in $E_{\rm Hartree}$. To see this, consider the one-sided Fourier transform of Eq. (13),

$$W(q,x) = \alpha\int dy e^{iqy}\left(\frac{1}{\sqrt{x^2+y^2}} - \frac{1}{\sqrt{x^2+y^2+4D^2}}\right) = \alpha[K_0(|qx|) - K_0(|q|\sqrt{4D^2+x^2})], \tag{24}$$

implying that $W(q\to 0,x)\simeq \alpha \ln\sqrt{1+[2D/x]^2}$. With these definitions, we obtain in a similar manner

$$\frac{\partial^2 E_{\rm Hartree}}{\partial \delta^2} = \frac{L}{\pi^2}[\eta(k_F,k_F) - \eta(k_F,-k_F) + \mathcal{R}]. \tag{25}$$

In view of Eqs. (16)–(25), only the magnitude of $\eta(k_F, -k_F)$ yields a nontrivial contribution to g at this level of approximation. Within the g-ology terminology,[3] we may identify this term with g_2, measuring the strength of forward scattering between particles of different directionality (henceforth referred to as chirality). On the other hand, scattering between equal-chirality particles is described by g_4, identified here as $\eta(k_F,k_F)$. However, according to Eqs. (20) and (25), an additional term $\mathcal{R}$ is present, which effectively modifies g_4. In 1D quantum wires with continuous (Galilean) translational invariance, both $n_k(x)$ and $\eta(k,k')$ are independent of k,k', and hence $\mathcal{R}=0$ and $\partial_\delta^2 E_{\rm Hartree}=0$. In that case, the Tomonaga-Luttinger liquid (TLL) parameter g depends only on the zero-momentum Fourier component of the interaction, $W(q\simeq 0)\approx \alpha \ln(D/d)$, where d is of the order of the wire width.

Similar (though slightly more involved) expressions can be found for the Fock contributions to Eq. (17), which are of the order $W(q\simeq 2k_F)$. Using Eq. (14), this amplitude can be estimated as

$$W(2k_F) \simeq \alpha\sqrt{\frac{\pi}{8k_F d}} e^{-4k_F d},$$

which is parametrically smaller than the Hartree amplitude. Similar to backscattering contributions, Fock contributions can thus safely be neglected against the Hartree terms for parameter regime (14).

B. TLL parameter estimate

In order to estimate the magnitude of the above terms, in particular of $\eta(k_F,-k_F)$, it is necessary to have some handle on the unperturbed wave functions $\phi_k(x)$ and $\chi_k(x)$, together with the resulting densities $n_k(x)$. We approximate their density profiles as

$$n_\kappa(\xi) \simeq \frac{(12b_0\kappa^2)^{1/8}}{\sqrt{\pi}} e^{-(12b_0\kappa^2)^{1/4}[\xi + \mathrm{sgn}(\kappa)\sqrt{\omega_B}d]^2}. \quad (26)$$

Note that the true densities describing snake orbits (see Fig. 4) are somewhat more complicated, with a double-peak shape. However, the simplified single-Gaussian form in Eq. (26) captures the essential physics and allows for analytical progress.

Given Eq. (26), introducing the lengthscale

$$\lambda = \left(\frac{3}{4}B_0\omega_B^2k_F^2\right)^{-1/8}, \quad (27)$$

and using Eq. (21), we are now in a position to estimate

$$\eta(k_F,-k_F) \simeq 8\alpha \ln(D/d),$$

$$\eta(k_F,k_F) \simeq 8\alpha \ln(e^{C/2}D/\lambda), \quad (28)$$

assuming $D \gg d \gg \lambda$ [see Eq. (14)]. Here $C=0.577\ldots$ is the Euler constant. We see that the ratio $\eta(k_F,-k_F)/\eta(k_F,k_F)$ approaches unity for $D\to\infty$ as in Galilei-invariant 1D wires, where in addition one also has $\mathcal{R}=0$. In order to estimate $\mathcal{R}$, we first observe that in Eq. (23), the $\eta(k,-k_F)$ term is suppressed by a factor $e^{-8(d/\lambda)^2}$ as compared to $\eta(k,k_F)$. This factor becomes small in regime (14), and we can therefore approximate $\mathcal{R} \simeq 2\int_0^{k_F} dk \partial_{k_F}\eta(k,k_F)$, which can be calculated in closed form for density profile (26),

$$\mathcal{R} \simeq 8\alpha[\sqrt{2}(c_1+2c_2) + 4(\sqrt{2}c_1-1)\ln(D/\lambda)]$$

$$\approx \alpha[5.73 - 2.60\ln(D/\lambda)]. \quad (29)$$

Employing the incomplete Euler Beta function, we find

$$c_1 = \frac{1}{3}\left(4\sqrt{2} - \int_0^1 dt \frac{\sqrt{1+t}}{t^{3/4}}\right) \simeq 0.6496 \quad (30)$$

and

$$c_2 = \int_0^1 dt \frac{t^{1/4}}{\sqrt{1+t}} \ln\left[\frac{1+t}{1+\sqrt{t}}\right] \simeq -0.07171. \quad (31)$$

Remarkably, $\mathcal{R}$ decreases with increasing D/λ, changes sign at $D \simeq 9.02\lambda$, and then continues to decrease logarithmically. Although asymptotically smaller by a factor $4(\sqrt{2}c_1-1) \simeq 0.326$ than the leading contribution [Eq. (28)] to g_4, the $\mathcal{R}$ term is important for quantitative estimates of the TLL parameter. For example, when $\mathcal{R}<0$, standard expressions (without $\mathcal{R}$) would overestimate g, pretending too weak interaction effects. The usual expressions are based on Galilei invariance, which is broken in the present system due to the periodic superstructure imposed on the 1D wire by the snake orbits. It is not obvious to us how standard estimates to g_4, starting from the microscopic interaction [Eq. (13)], would recover the $\mathcal{R}$ contribution.

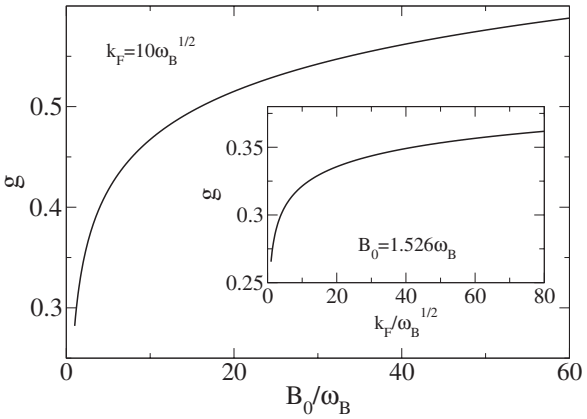

FIG. 5. TLL parameter g in Eq. (32) for $\alpha=1$ and $D=100/\sqrt{\omega_B}$. Main panel: g as a function of B_0/ω_B for $k_F=10\sqrt{\omega_B}$. Inset: g vs $k_F/\sqrt{\omega_B}$ for $B_0=1.526\omega_B$. Note that the regime $\lambda \ll d$ translates into $k_F \gg \frac{18}{\sqrt{3}}\omega_B^2 B_0^{-5/2}$, which here implies $k_F/\sqrt{\omega_B} > 1$.

Combining Eqs. (16)–(29), we get the analytical estimate for the TLL parameter,

$$g \simeq \left[\frac{g_0 - \ln(D/d)}{g_0 + \ln(D/d)}\right]^{1/2}, \quad (32)$$

in the regime $D \gg d \gg \lambda$ [see Eq. (14)], where λ is given in Eq. (27). Here, we have abbreviated

$$g_0 = \frac{\pi}{2\alpha} + \sqrt{2}(c_1+2c_2) + 4(\sqrt{2}c_1-1)\ln\frac{D}{\lambda} + \ln\left(e^{C/2}\frac{D}{\lambda}\right). \quad (33)$$

TLL parameter (32) is depicted in Fig. 5, where $|\partial_k \varepsilon_{k_F}| = v_F$ and a "fine structure constant" $\alpha=1$ have been assumed. However, according to Eq. (33), changes in α may be compensated for via changes in λ, i.e., by modification of k_F or of the magnetic-field parameters.

As shown in the inset of Fig. 5, values of about $g \approx 0.3$ are expected for the chosen value of B_0, with no pronounced variations when changing D/λ. Such weak sensitivity to k_F found in graphene is in stark contrast to semiconducting wires, where g can vary significantly when changing the carrier density.[44] As discussed in Sec. I, similar values for g as compared to the values in Fig. 5 have been reported for other TLL systems such as quantum wires[8] or single-wall nanotubes (SWNTs).[9,32,33] On the other hand, the main panel in Fig. 5 demonstrates that g can be widely tuned in graphene wires by changing the snake-state separation $2d$ in Eq. (7) via the magnetic-field parameters, in particular by sweeping the background field B_0.

V. CONCLUSIONS

In this paper, we have analyzed the effects of electron-electron interactions on the electronic properties of magnetic waveguides formed in suitable inhomogeneous magnetic fields in graphene. When there are two parallel lines along which the magnetic field vanishes, a pair of counterpropagating snake states can be formed, which are ideal unidirec-

tional (chiral) channels similar to the edge states in quantum Hall bars. We have studied the case of a smooth magnetic-field profile across the wire, but similar results are expected also for other profiles, e.g., for piece-wise constant fields. Employing a combination of analytical methods for the band structure and for the eigenfunctions (which were checked against exact diagonalization results) with a thermodynamical approach, we have obtained a closed result for the nonuniversal TLL parameter [see Eq. (32) and Fig. 5]. This parameter then determines the power-law exponents appearing in many observables of interest, in particular in the energy-dependence of the tunneling density of states. Quite remarkably, we have uncovered that the snake orbits impose a periodic superstructure that breaks Galilei invariance of the resulting wire, and modifies the commonly used estimate for the TLL parameter g. The finite $\mathcal{R}$ term in Eq. (29) reflects this physics. We expect this correction to affect also edge states in quantum Hall bars. Typical values for g found here are comparable to the values reported for semiconductor quantum wires and single-wall carbon nanotubes. We thus expect that non-Fermi liquid behavior should be sufficiently pronounced to be observable in systems based on inhomogeneous magnetic fields.

There are two main advantages regarding experimental observability in our system when compared to previous TLL realizations. First, the TLL parameter g can be tuned over a significant region by sweeping the strength of the homogeneous part of the magnetic profile. This is illustrated in the main panel of Fig. 5. Second, the unavoidable presence of disorder is not expected to affect the TLL behavior since right- and left-moving electrons are spatially separated. This may allow to experimentally study the physics of an ultraclean TLL state.

While there are similarities to the physics of quantum Hall edge states, the TLL state discussed here is quite different from the chiral Luttinger liquid discussed in the context of the fractional quantum Hall effect.[42] The g parameter in the latter case is fixed by the bulk filling factor, while here it is nonuniversal and tunable. From a conceptual point of view, the quantum Hall situation is also more intricate because of the coupling of edge states to bulk states.[42] Such complications are absent for the TLL state discussed in this paper. To conclude, we hope that our work motivates experiments in this direction.

ACKNOWLEDGMENTS

We thank T. Heinzel for discussions. W.H. would like to thank H. Grabert for continuous support. This work has been supported by the SFB-TR/12, by the ESF INSTANS program, and by the A. v. Humboldt foundation.

APPENDIX: NUMERICAL DIAGONALIZATION

In this appendix, we provide some details on how the numerical diagonalization mentioned in Sec. II B has been implemented. From Eq. (6), we first observe that exact eigenfunctions $\phi(x)$ of Eq. (3) behave as $\sim\exp[-\frac{x^{1+\nu}}{1+\nu}]$ for $x\to\infty$. For example, the exact zero-energy state to Eq. (9) is given as $(e^{-\xi^4/4+b_0\xi^2/2+\kappa\xi},0)^T$ up to a normalization factor.

However, it is clear that accurate eigenvalues ε_k^2 only require to maximize the overlap between the approximated wave function and $\phi(x)$. For convenience, we thus use the complete and orthonormal oscillator basis

$$\varphi_n(\xi)=\frac{1}{\pi^{1/4}\sqrt{2^n n!}}e^{-\xi^2/2}H_n(\xi),$$

where H_n are Hermite polynomials. Matrix elements of the operator H^2 in Eq. (3) in this basis read ($b_0=B_0/\omega_B$)

$$\begin{aligned}\omega_B^{-1}\langle\varphi_n|H^2|\varphi_{n'}\rangle=&(2n+1+\kappa^2)\delta_{nn'}+\langle\varphi_n|\xi^{2\nu}-(1-b_0^2)\xi^2\\&-2b_0\xi^{\nu+1}|\varphi_{n'}\rangle-\langle\varphi_n|2k(\xi^\nu-b_0\xi)\\&-\tau_z(\nu\xi^{\nu-1}-b_0)|\varphi_{n'}\rangle,\end{aligned}$$

where we use that for integer γ and even $n+n'+\gamma$ (Γ denotes the Gamma function)

$$\begin{aligned}\langle\varphi_n|\xi^\gamma|\varphi_{n'}\rangle=&\sqrt{\frac{2^{n+n'}n!\,n'!}{\pi}}\sum_{m=0}^{[n/2]}\sum_{m'=0}^{[n'/2]}\left(-\frac{1}{4}\right)^{m+m'}\\&\times\frac{\Gamma\left(\frac{1+n+n'+\gamma}{2}-m-m'\right)}{m!\,m'!\,(n-2m)!\,(n'-2m')!},\end{aligned}$$

where $\langle\varphi_n|\xi^\gamma|\varphi_{n'}\rangle=0$ otherwise. The symbol $[n]$ denotes the largest integer smaller or equal to n. Upon carrying out standard diagonalization for $0\le n,\ n'\le 30$ basis functions, we obtain the energy dispersion ε_k in Figs. 1 and 3 for $\nu=2$ and $\nu=3$, respectively. To numerical accuracy, all levels are found independent of $\tau_z=\pm 1$, although the effective potentials in Eq. (3) differ considerably. Only the zero-energy level $\varepsilon_k=0$ in Fig. 3 (there is no zero-energy level in Fig. 1) belongs purely to the upper pseudospin component $\tau_z=+1$ for the valley point K chosen here. With the numerical diagonalization, we also obtain the eigenfunctions $\phi_k(x)$ and $\chi_k(x)$ of the Dirac Hamiltonian [Eq. (2)]. In Figs. 2 and 4, we show the resulting density profiles for $\nu=2$ and $\nu=3$, respectively. All figures nicely confirm the overall picture developed in Sec. II B.

[1] For reviews, see e.g., *Quantum Transport in Ultrasmall Devices*, NATO Advanced Studies Institute, Series B: Physics Vol. 342, edited by D. K. Ferry (Plenum, New York, 1995).

[2] *Carbon Nanotubes: Synthesis, Structure, Properties, and Applications*, Springer Topics in Applied Physics Vol. 80, edited by M. S. Dresselhaus, G. Dresselhaus, and Ph. Avouris (Springer, Berlin, 2001).

[3] J. Sólyom, Adv. Phys. **28**, 201 (1979).

[4] F. D. M. Haldane, J. Phys. C **14**, 2585 (1981).
[5] J. Voit, Rep. Prog. Phys. **57**, 977 (1994).
[6] A. O. Gogolin, A. A. Nersesyan, and A. M. Tsvelik, *Bosonization and Strongly Correlated Systems* (Cambridge University Press, Cambridge, England, 1998).
[7] T. Giamarchi, *Quantum Physics in One Dimension* (Oxford University Press, New York, 2003).
[8] For very recent experimental reports on TLL behavior in semiconductor quantum wires, see H. Steinberg, G. Barak, A. Yacoby, L. N. Pfeiffer, K. W. West, B. I. Halperin, and K. Le Hur, Nat. Phys. **4**, 116 (2008), and references therein.
[9] M. Bockrath, D. H. Cobden, J. Lu, A. G. Rinzler, R. E. Smalley, L. Balents, and P. L. McEuen, Nature (London) **397**, 598 (1999); Z. Yao, H. W. Ch. Postma, L. Balents, and C. Dekker, *ibid.* **402**, 273 (1999); B. Gao, A. Komnik, R. Egger, D. C. Glattli, and A. Bachtold, Phys. Rev. Lett. **92**, 216804 (2004).
[10] K. S. Novoselov, A. K. Geim, S. V. Morozov, D. Jiang, Y. Zhang, S. V. Dubonos, I. V. Grigorieva, and A. A. Firsov, Science **306**, 666 (2004); K. S. Novoselov, A. K. Geim, S. V. Morozov, D. Jiang, M. I. Katsnelson, I. V. Grigorieva, S. V. Dubonos, and A. A. Firsov, Nature (London) **438**, 197 (2005); Y. Zhang, Y.-W. Tan, H. L. Stormer, and P. Kim, *ibid.* **438**, 201 (2005); C. Berger, Z. Song, X. Li, X. Wu, N. Brown, C. Naud, D. Mayou, T. Li, J. Hass, A. N. Marchenkov, E. H. Conrad, P. N. First, and W. A. de Heer, Science **312**, 1191 (2006); F. Molitor, J. Güttinger, C. Stampfer, D. Graf, T. Ihn, and K. Ensslin, Phys. Rev. B **76**, 245426 (2007).
[11] For a review, see A. K. Geim and K. S. Novoselov, Nat. Mater. **6**, 183 (2007).
[12] We absorb the factor e/c into A and B.
[13] G. W. Semenoff, Phys. Rev. Lett. **53**, 2449 (1984); D. P. DiVincenzo and E. J. Mele, Phys. Rev. B **29**, 1685 (1984).
[14] F. M. Peeters and A. Matulis, Phys. Rev. B **48**, 15166 (1993); N. Malkova, I. Gómez, and F. Domínguez-Adame, *ibid.* **63**, 035317 (2001); S. M. Badalyan and F. M. Peeters, *ibid.* **64**, 155303 (2001); J. M. Pereira, Jr., F. M. Peeters, and P. Vasilopoulos, *ibid.* **75**, 125433 (2007).
[15] S. J. Lee, S. Souma, G. Ihm, and K. J. Chang, Phys. Rep. **394**, 1 (2004).
[16] A. De Martino, L. Dell'Anna, and R. Egger, Phys. Rev. Lett. **98**, 066802 (2007).
[17] M. Ramezani Masir, P. Vasilopoulos, A. Matulis, and F. M. Peeters, Phys. Rev. B **77**, 235443 (2008).
[18] J. E. Müller, Phys. Rev. Lett. **68**, 385 (1992); J. Reijniers and F. M. Peeters, J. Phys.: Condens. Matter **12**, 9771 (2000); J. Reijniers, A. Matulis, K. Chang, F. M. Peeters, and P. Vasilopoulos, Europhys. Lett. **59**, 749 (2002); H. Xu, T. Heinzel, M. Evaldsson, S. Ihnatsenka, and I. V. Zozoulenko, Phys. Rev. B **75**, 205301 (2007).
[19] P. D. Ye, D. Weiss, R. R. Gerhardts, M. Seeger, K. von Klitzing, K. Eberl, and H. Nickel, Phys. Rev. Lett. **74**, 3013 (1995); D. Lawton, A. Nogaret, M. V. Makarenko, O. V. Kibis, S. J. Bending, and M. Henini, Physica E (Amsterdam) **13**, 699 (2002); M. Hara, A. Endo, S. Katsumoto, and Y. Iye, Phys. Rev. B **69**, 153304 (2004); M. Cerchez, S. Hugger, T. Heinzel, and N. Schulz, *ibid.* **75**, 035341 (2007).
[20] L. Oroszlány, P. Rakyta, A. Kormányos, C. J. Lambert, and J. Cserti, Phys. Rev. B **77**, 081403(R) (2008).
[21] T. K. Ghosh, A. De Martino, W. Häusler, L. Dell'Anna, and R. Egger, Phys. Rev. B **77**, 081404(R) (2008).
[22] A. Kormányos, P. Rakyta, L. Oroszlány, and J. Cserti, Phys. Rev. B **78**, 045430 (2008).
[23] H.-W. Lee and D. S. Novikov, Phys. Rev. B **68**, 155402 (2003); N. Nemec and G. Cuniberti, *ibid.* **74**, 165411 (2006).
[24] In thermal equilibrium, unidirectional 1D states must occur in pairs of counterpropagating snake (or edge) modes (Refs. 20 and 21).
[25] A. Nogaret, S. J. Bending, and M. Henini, Phys. Rev. Lett. **84**, 2231 (2000).
[26] A. Bostwick, T. Ohta, T. Seyller, K. Horn, and E. Rotenberg, Nat. Phys. **3**, 36 (2007).
[27] M. O. Goerbig, R. Moessner, and B. Douçot, Phys. Rev. B **74**, 161407(R) (2006); K. Nomura and A. H. MacDonald, Phys. Rev. Lett. **96**, 256602 (2006); L. Sheng, D. N. Sheng, F. D. M. Haldane, and L. Balents, *ibid.* **99**, 196802 (2007); C.-H. Zhang and Y. N. Joglekar, Phys. Rev. B **75**, 245414 (2007).
[28] T. Ando, J. Phys. Soc. Jpn. **75**, 074716 (2006); V. V. Cheianov and V. I. Fal'ko, Phys. Rev. Lett. **97**, 226801 (2006); E. G. Mishchenko, *ibid.* **98**, 216801 (2007); Y. Barlas, T. Pereg-Barnea, M. Polini, R. Asgari, and A. H. MacDonald, *ibid.* **98**, 236601 (2007); E. Mariani, L. I. Glazman, A. Kamenev, and F. von Oppen, Phys. Rev. B **76**, 165402 (2007).
[29] J. Gonzalez, F. Guinea, and M. A. H. Vozmediano, Nucl. Phys. B **424**, 595 (1994); Phys. Rev. B **63**, 134421 (2001); T. Stauber, F. Guinea, and M. A. H. Vozmediano, *ibid.* **71**, 041406(R) (2005); D. T. Son, *ibid.* **75**, 235423 (2007).
[30] I. F. Herbut, Phys. Rev. Lett. **97**, 146401 (2006); D. V. Khveshchenko, Phys. Rev. B **74**, 161402(R) (2006); S. Das Sarma, E. H. Hwang, and W.-K. Tse, *ibid.* **75**, 121406 (2007); I. F. Herbut, V. Juricic, and O. Vafek, Phys. Rev. Lett. **100**, 046403 (2008).
[31] H. A. Fertig and L. Brey, Phys. Rev. Lett. **97**, 116805 (2006); M. Zarea and N. Sandler, *ibid.* **99**, 256804 (2007).
[32] R. Egger and A. O. Gogolin, Phys. Rev. Lett. **79**, 5082 (1997); C. Kane, L. Balents, and M. P. A. Fisher, *ibid.* **79**, 5086 (1997).
[33] R. Egger and A. O. Gogolin, Eur. Phys. J. B **3**, 281 (1998).
[34] I. Safi and H. J. Schulz, Phys. Rev. B **52**, R17040 (1995).
[35] B. Trauzettel, R. Egger, and H. Grabert, Phys. Rev. Lett. **88**, 116401 (2002); F. Dolcini, B. Trauzettel, I. Safi, and H. Grabert, Phys. Rev. B **71**, 165309 (2005).
[36] L. C. Biedenharn, Phys. Rev. **126**, 845 (1962); G. J. Papadopoulos and J. T. Devreese, Phys. Rev. D **13**, 2227 (1976); M. A. Kayed and A. Inomata, Phys. Rev. Lett. **53**, 107 (1984); T. Boudjedaa, L. Chetouani, L. Guechi, and T. F. Hammann, Phys. Scr. **46**, 289 (1992).
[37] P. Carmier and D. Ullmo, arXiv:0801.4727 (unpublished).
[38] Y. Aharonov and A. Casher, Phys. Rev. A **19**, 2461 (1979); L. Erdös and V. Vougalter, Commun. Math. Phys. **225**, 299 (2002).
[39] S. Park and H.-S. Sim, Phys. Rev. B **77**, 075433 (2008).
[40] I. E. Dzyaloshinskiĭ, and A. I. Larkin, Zh. Eksp. Teor. Fiz. **65**, 411 (1973) [Sov. Phys. JETP **38**, 202 (1974)].
[41] B. I. Halperin, Phys. Rev. B **25**, 2185 (1982); A. H. MacDonald, Phys. Rev. Lett. **64**, 220 (1990).
[42] A. M. Chang, Rev. Mod. Phys. **75**, 1449 (2003).
[43] U. Zülicke and A. H. MacDonald, Phys. Rev. B **54**, 16813 (1996).
[44] W. Häusler, L. Kecke, and A. H. MacDonald, Phys. Rev. B **65**, 085104 (2002).
[45] J. Alicea and M. P. A. Fisher, Phys. Rev. B **74**, 075422 (2006).
[46] H. P. Dahal, Y. N. Joglekar, K. S. Bedell, and A. V. Balatsky, Phys. Rev. B **74**, 233405 (2006).

[47] C. E. Creffield, W. Häusler, and A. H. MacDonald, Europhys. Lett. **53**, 221 (2001).
[48] G. Ernst, N. B. Zhitenev, R. J. Haug, and K. von Klitzing, Phys. Rev. Lett. **79**, 3748 (1997).
[49] This also applies to multiband situations, cf. W. Häusler, Phys. Rev. B **70**, 115313 (2004).
[50] E. Lieb and F. Y. Wu, Phys. Rev. Lett. **20**, 1445 (1968).
[51] N. Kawakami and S.-K. Yang, Phys. Rev. Lett. **67**, 2493 (1991).
[52] L. Kecke and W. Häusler, Phys. Rev. B **69**, 085103 (2004).